

Received March 22, 2022, accepted April 22, 2022, date of publication April 25, 2022, date of current version May 5, 2022.

Digital Object Identifier 10.1109/ACCESS.2022.3170451

# Enhancing Electrocaloric Heat Pump Performance by Over 99% Efficient Power Converters and Offset Fields

STEFAN MOENCH<sup>1</sup>, (Member, IEEE), RICHARD REINER<sup>1</sup>, PATRICK WALTEREIT<sup>1</sup>, CHRISTIAN MOLIN<sup>2</sup>, SYLVIA GEBHARDT<sup>2</sup>, DAVID BACH<sup>3</sup>, ROLAND BINNINGER<sup>3</sup>, AND KILIAN BARTHOLOMÉ<sup>3</sup>

<sup>1</sup>Fraunhofer Institute for Applied Solid State Physics (Fraunhofer IAF), 79108 Freiburg, Germany

<sup>2</sup>Fraunhofer Institute for Ceramic Technologies and Systems (Fraunhofer IKTS), 01277 Dresden, Germany

<sup>3</sup>Fraunhofer Institute for Physical Measurement Techniques (Fraunhofer IPM), 79110 Freiburg, Germany

Corresponding author: Stefan Moench (stefan.moench@iaf.fraunhofer.de)

This work was supported by the Fraunhofer Society through the Fraunhofer Lighthouse Project EIKaWe (www.EIKaWe.org).

**ABSTRACT** This work analyzes how an over 99% efficient charging circuit and electrical offset fields enhance the coefficient of performance (COP) of electrocaloric heat pumps, an emerging technology with zero global warming potential. The COP is studied for Carnot-like cycles regarding the material's permittivity and dissipation factor, and the system's charging efficiency. Compared to the Carnot limit, a relative material COP of 50.4% is calculated for a lead magnesium niobate (PMN) ceramic, and enhanced to 87.4% by an offset field. The offset avoids high loss at low fields, where the non-linear permittivity-related dissipative loss is highest. A 99.2% efficient gallium nitride half-bridge switched-mode converter is used as charging circuit. Including the charging loss, the calculated relative system COP of 11.9% is significantly enhanced to 28.6% by an offset field. The 0.8% external loss exceeds the material loss (dissipation factor below 0.2%), reducing the system COP from the material COP. Compared to 80% efficient state-of-the-art resonant circuits for electrocalorics, this work's approach reduced charging loss 20 times. The work contributes to transfer the high COP of electrocaloric materials also to electrocaloric heat pump systems.

**INDEX TERMS** Electrocalorics, heat pumps, coefficient of performance, power conversion, pyroelectric devices, dielectric losses, energy efficiency, thermal analysis, circuit analysis.

## I. INTRODUCTION

### A. BACKGROUND

Electrocaloric (EC) multilayer ceramic capacitors (MLCCs) based on lead magnesium niobate (PMN) [1]–[3] are promising components for emerging efficient heat pumps and cooling or heating systems with zero global warming potential [4]. Fig. 1 shows the four phases of a Carnot-like cycle, where the temperature of the electrocaloric material is reversibly changed by applying and removing an external field. With alternating thermal contact to either a heat sink or source (hot side and cold side) a heat-pump is created where heat  $Q_C$  is absorbed from the cold side. The heat pump is usable for heating or cooling applications, and the cooling configuration is exemplary analyzed in this work without limiting the generality of the analysis.

The associate editor coordinating the review of this manuscript and approving it for publication was Jie Tang.

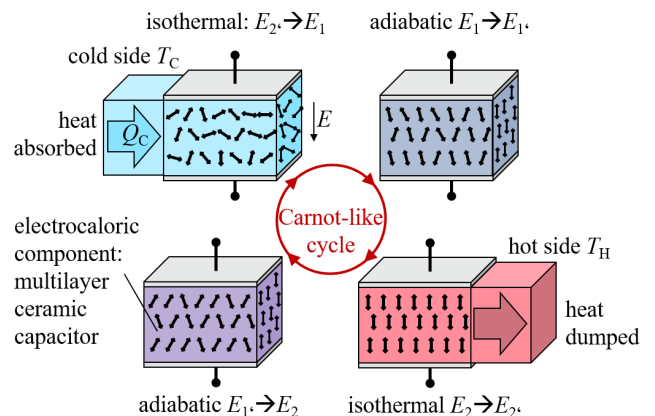


**FIGURE 1.** Carnot-like cycle with electrocaloric component, alternating between a heat source and sink. The varying electric field  $E$  causes a mostly reversible temperature  $T$  change in adiabatic phases (electrocaloric effect) and heat flow in isothermal phases.

Considering only the high and reversible electrocaloric adiabatic temperature change  $\Delta T_{AD,MAX}$  (typ.  $> 1$  K), it seems

that a high material coefficient of performance (COP)

$$COP_{MAT} = \frac{\dot{Q}_C}{P_{EL,INT}}, \quad (1)$$

which describes the ratio of pumped thermal cooling power output  $\dot{Q}_C$  to electrical input power  $P_{EL,INT}$ , close to the Carnot limit is theoretically achievable [5]. This high material performance limit (ignoring the required external system loss) results if the internal material loss is very low. This is the case for example for electrocaloric ceramics with dissipation factors  $DF$  as low as  $<0.2\%$ , despite the very high permittivity ( $\epsilon_R > 1000 \dots 10000$ ) of the ceramic material.

The high permittivity however causes a high reactive charging and discharging power required to change the voltage across the capacitor and thus the electric field in the dielectric to cause the EC effect. Even though most of the stored energy in the EC capacitor can be recovered, the external circuit has to provide this high reactive charging/discharging power. To provide the reactive charging power, the power is converted externally, which causes additional power loss proportional to the charging power. The external charging loss is part of complete heat pump systems, and decisive for the performance of complete heat pump systems, because the additional external charging loss  $P_{EL,EXT}$  reduces the performance from the material limit to the lower system coefficient of performance

$$COP_{SYS} = \frac{\dot{Q}_C}{P_{EL,INT} + P_{EL,EXT}}. \quad (2)$$

The importance of electric-energy recovery for maintaining a high performance also on the system level is highlighted in [5]. Fig. 2a shows a schematic of the electrical and thermal power flow with the material and system coefficients of performance, the reactive charging power and a charging circuit with efficiency  $\eta_{DC}$ .

Fig. 2b shows a generic configuration where one electrocaloric capacitor is charged and discharged to a buffer capacitor. The electric field in the EC material results from the output voltage of the charging circuit  $V_C$ , and can either be operated starting from a zero field, or from an offset field. Fig. 2c shows a generic configuration where two similar electrocaloric capacitors are charged and discharged without a buffer capacitor. While both configurations can achieve the same electrical efficiency, the second configuration does not require large buffer capacitors, improving the power density of the charging circuit. However, in this work the focus is on maximizing the efficiency and not power density, and thus the first configuration (Fig. 2a) is used in the following.

As indicated in Fig. 2a, the material COP is limited only by material parameters, namely the magnitude of EC effect ( $\Delta T/\Delta E$ ), the permittivity  $\epsilon$  and dissipation factor  $DF$  (in addition to the density  $\rho$  and heat capacity  $c_p$ ).

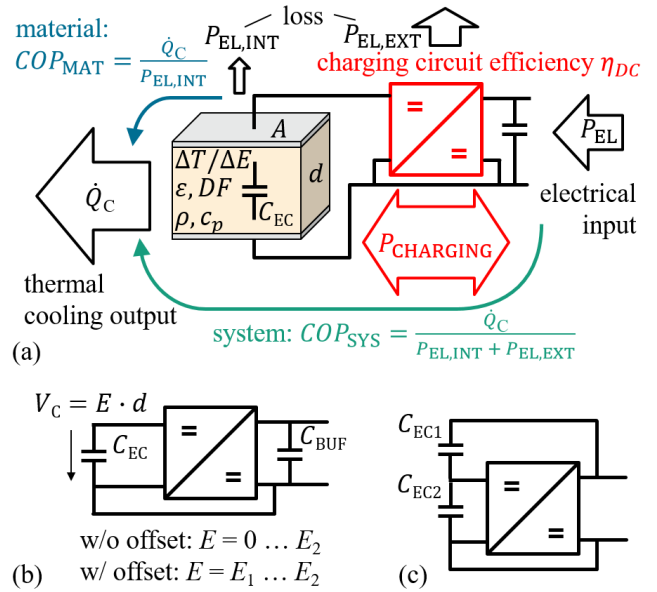


**FIGURE 2.** (a) Schematic of charging circuit and the coefficient of performance (COP) between the electrical input and pumped thermal output power. (b) Configuration with one EC capacitor and a buffer capacitor. (c) Configuration with two EC capacitors.

The system COP on the other hand is additionally limited by the external parameter of charging circuit efficiency  $\eta_{DC}$ .

### 1) EFFICIENT CHARGING CIRCUITS FOR IMPROVED SYSTEM PERFORMANCE

It was already recognized that highly-efficient charging circuits are “needed to achieve competitive system efficiency” [6]. Charge recovery circuits based on resonant circuits have been used in literature for electrocaloric capacitors to recover around 80% [7], [8] of the stored energy. Further circuits might be adapted from known circuits for piezoelectric actuator drivers [9], [10]. This state-of-the-art charge recovery circuits for electrocaloric capacitors can be replaced by highly-efficient bi-directional switched-mode power supplies (SMPS). Switched-mode power supplies are known for very high achievable efficiencies [11] compared to resonant circuits. However, such power converters have not yet been applied to electrocaloric applications.

### 2) OFFSET FIELDS FOR IMPROVED MATERIAL PERFORMANCE

While operation of the electrocaloric material between zero and a maximum field gives the highest absolute temperature effect, operation starting at an offset avoids the high permittivity range of the ceramic at low fields and reduces the required reactive charging power significantly and more than the reduction of the temperature effect. Thus, operation of EC ceramics with offset field allows a significant improvement of the best-case system COP. Experimentally, the improvement by an offset field was observed in [8], but not further

systematically analyzed or exploited. The reduced absolute temperature change, if an offset is used, can be compensated by cascading [12]–[14] more EC elements in series using an appropriate system approach.

## B. PROBLEM

This work addresses two problems of electrocaloric heat pumps which limit the up to now achieved system coefficient of performance:

- State-of-the-art charge recovery circuits used so far for electrocaloric prototypes are based on resonant circuits and reported efficiencies of up to 80% are low, significantly reducing the system performance from the material limit.
- Material performance improvement using offset fields was experimentally observed, but has not yet been systematically analyzed and exploited.

## C. APPROACH

This work investigates how the external charging efficiency and an offset field for low-loss electrocaloric ceramics improve the best-case system coefficient of performance.

First, the relationship between the non-linear permittivity and loss factor, stored energy, material and external loss is analytically described.

Then, this work uses an up to 99.2% efficient gallium nitride (GaN)-based half-bridge converter published by the authors in [15] as a charging circuit for the electrocaloric PMN sample during continuous operation. The converter is optimized and used to experimentally operate an electrocaloric PMN sample with different offset fields.

From the measured reactive charging power, active power loss and measured adiabatic temperature change on the sample, the best-case system COPs and figure-of-merits (FOMs) are calculated to demonstrate the beneficial effect of offset fields and the high charging efficiency.

## D. ELECTROCALORIC SAMPLE PREPARATION AND CHARACTERIZATION

The PMN MLCC used in this work was fabricated according to the procedure described in [2]. Fig. 3 shows a photo of the electrocaloric PMN MLCC sample.

Fig. 4 (solid lines) shows the measured relative permittivity  $\epsilon_R$ , loss factor  $DF$  (using an LCR-meter) as function of the applied field  $E$ , and the electrocaloric temperature change  $\Delta T_{AD,MAX}$  for field changes from zero to  $E$  for a PMN MLCC sample at room temperature. As reasoned in [2], the internal material  $\Delta T_{AD,MAX}$  (dotted lines) is higher than the measured values (solid) by a ratio of  $k_T$ . This ratio is due to ratio of the thickness and materials of the electrodes compared to the active EC layers and can be reduced. The permittivity (of ceramics) is highly non-linear depending on the applied electrical field and decreases more than 10-times compared to the zero field permittivity.

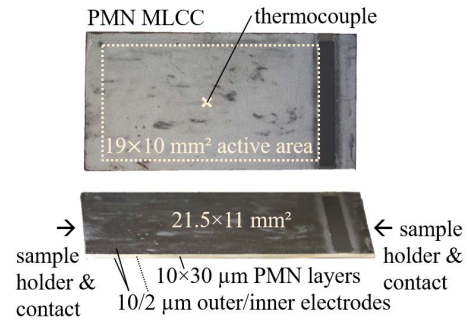


FIGURE 3. Foto and geometry of PMN MLCC sample.

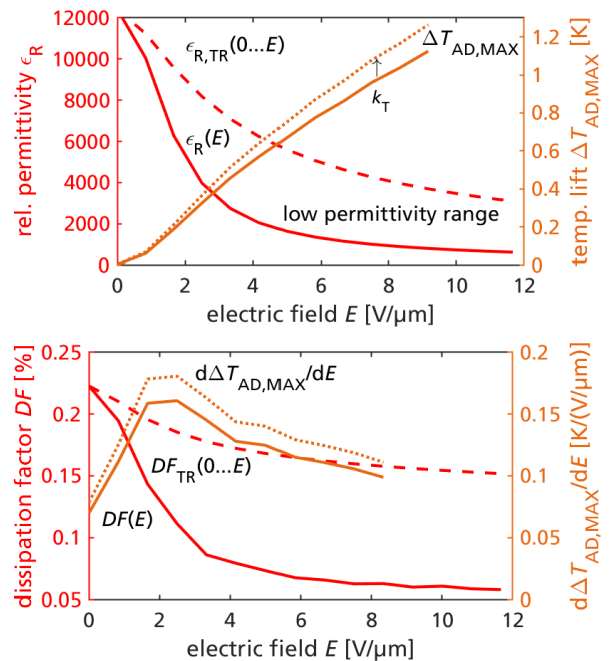


FIGURE 4. Field-dependent permittivity  $\epsilon_R(E)$  (top) and dissipation-factor  $DF(E)$  (bottom) for a PMN sample. Electrocaloric temperature change  $\Delta T_{AD,MAX}$  (top) and change thereof (bottom). Solid: At the field  $E$ . Dashed: Effective  $\epsilon_{TR}(0 \dots E)$ ,  $DF_{TR}(0 \dots E)$  during operation between  $0 \dots E$ . The internal  $\Delta T_{AD,MAX}$  (dotted) is higher by a factor  $k_T$  than the measured surface temperatures (solid).

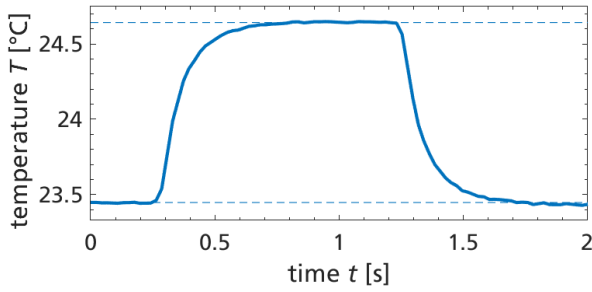
The observed electrocaloric adiabatic temperature change per field change  $d\Delta T_{AD,MAX}/dE$  however only decreases slightly with increasing electrical field  $E$ .

Fig. 5 shows an exemplary temperature measurement at 0.5 Hz for a field change of 10 V/µm during continuous adiabatic operation. The two temperature state levels (dashed) are extracted using the histogram method.

## II. ANALYSIS OF ELECTROCALORIC COOLING CYCLE

### A. THERMAL CYCLE

A Carnot-like cycle is analyzed as the best practically achievable thermal cycle. Fig. 6 shows the temperature and electric field during the four phases of the cycle. This Carnot-like cycle deviates from a true Carnot-cycle due to the low



**FIGURE 5.** Adiabatic temperature measurement at 0.5 Hz and 300 V (10V/ $\mu\text{m}$ ) at room temperature with zero offset. The state levels (dashed) are extracted with the histogram method. (raw data, not corrected by  $k_T$ ).

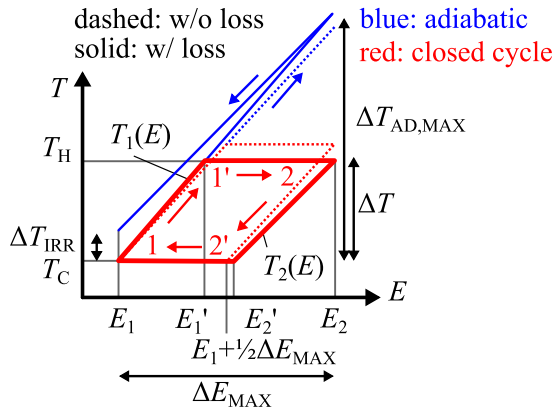


**FIGURE 6.** The analyzed Carnot-like thermal cycle (solid lines) with adiabatic (1-1', 2-2') and isothermal phases (1'-2, 2'-1) differs from a Carnot cycle (dashed) due to non-reversible dissipation in the electrocaloric material.

non-reversible dissipation which is caused by the dissipation factor of the material during charging and discharging times. First, from the low field  $E_1$  (either zero, or the later investigated offset field) and cold temperature  $T_C$ , the electric field is increased under adiabatic conditions to the field  $E'_1$  where the hot temperature  $T_H$  is just reached. Then, under isothermal conditions, the field is further increased to  $E_2$  while heat is dumped into the hot side. Next, under adiabatic conditions, the field is reduced to  $E'_2$  by part of the full field change  $\Delta E = E_2 - E_1$  with the ratio

$$a' = \frac{E_2 - E'_2}{\Delta E}, \quad (3)$$

such that the cold temperature is just reached again. Last, the field is further reduced to  $E_1$  under adiabatic conditions, while heat  $Q_C$  is absorbed from the cold side.

The temperature difference  $\Delta T = T_H - T_C < \Delta T_{AD,MAX}$  is reduced from the adiabatic temperature for the same field change if heat is absorbed  $Q_C > 0$  such as in useful thermal cycles. The optimal  $\Delta T$  (and associated optimal  $E'_1, E'_2$ ) for the highest relative coefficient of performance  $COP_R$ , occurs approximately at temperature difference  $\Delta T \approx \frac{1}{2} \Delta T_{AD,MAX}$  (or field ratio  $a' \approx \frac{1}{2}$ ) for the analyzed Carnot-like cycle, as also shown in [6] and [16] and is calculated later in this paper.

## B. THERMAL ANALYSIS

The linearized thermal coupling equation [6] for electrocalorics, normalized to volume, is extended in this work by the irreversible dissipation in the dielectric as

$$dQ = pT dE + \rho c_P dT - \frac{\pi}{8} DF_{TR} \varepsilon_{TR} \Delta E_{MAX} |dE|, \quad (4)$$

with the measured pyroelectric coefficient

$$p = -\frac{\rho c_P}{T} \frac{\Delta T_{AD,MAX}}{\Delta E_{MAX}} < 0, \quad (5)$$

an electric field  $E \geq 0$  in unipolar operation, the effective permittivity  $\varepsilon_{TR}$  and the effective dissipation factor  $DF_{TR}$ . The modulus  $|dE|$  describes the non-reversibility of the dielectric losses as the electric field changes. For a simplified analysis, the effect of the dielectric loss factor which is typically measured for a sinusoidal signal at a frequency  $f$  where neither the leakage current nor the series resistance of the sample is dominant (here 1 kHz) is linearized such that the calculated total non-reversible heating which is  $\frac{\pi}{4} DF_{TR} \varepsilon_{TR} \Delta E_{MAX}^2$ , calculated from the last term in Eqn. 4 for a complete cycle (charging and then discharging with a constant slope of  $dE/dt$ , such that the summed up field change change is  $2\Delta E$ ) is equal to the dissipation for a sinusoidal excitation with an amplitude of  $\pm \frac{1}{2} \Delta E$  and the measured  $DF$ . The factor  $\frac{1}{8}$  (instead of  $\frac{1}{2}$ ) is explained because the electrocaloric element is operated with unipolar fields, and typically the (peak-to-peak) field change  $\Delta E$  is used in calculations, which is twice the amplitude  $\frac{1}{2} \Delta E$  of a hypothetical bipolar (sinusoidal) signal.

It is noted that this work summarizes the material loss in the equivalent dissipation factor  $DF_{TR}$ , based on the bias-dependent small-signal measurement data. In the case of the investigated PMN material the result is verified later in this paper by large-signal measurements. However, some other electrocaloric materials such as polymers or ceramics with significant hysteresis or ferroelectric effects might have higher loss during large-signal operation than calculated from small-signal measurements. In that case,  $DF_{TR}$  should be extracted from large-signal power loss measurements. For simplicity, the material density  $\rho$  and specific heat capacity  $c_P$  are considered constant, and the effective time-related (TR) permittivity  $\varepsilon_{TR}$  and dissipation factor  $DF_{TR}$

$$\varepsilon_{TR} = \frac{1}{\Delta E_{MAX}} \int_{E_1}^{E_2} \varepsilon(E) dE, \quad (6)$$

$$DF_{TR} = \frac{1}{\Delta E_{MAX} \varepsilon_{TR}} \int_{E_1}^{E_2} \varepsilon(E) DF(E) dE. \quad (7)$$

with  $E_2 = E_1 + \Delta E_{MAX}$  are used to condense the E-field dependent  $\varepsilon(E)$  and  $DF(E)$ .  $\Delta T_{AD,MAX}$  denotes the adiabatic temperature change of the active electrocaloric material during continuous cyclic adiabatic operation with an electric field change of  $\Delta E_{MAX}$  and sufficiently low frequency to allow settling of the two measured transient temperature levels. The indicator *MAX* denotes adiabatic conditions, in contrast to the operation with reduced temperature differences

during actual useful thermal cycles. The electrodes of the MLCC component add additional mass which reduces the effective externally observed temperature change. For a typical MLCC with  $N$  electrocaloric ceramic layers between 2 outer and  $N - 1$  inner electrodes, the transformation coefficient [2]

$$k_T = \frac{N\rho_{cp}t + (N-1)\rho_{Icp}t_I + 2\rho_{Ocp}t_O}{N\rho_{cp}t} \geq 1 \quad (8)$$

is used to determine the internal temperature change  $\Delta T_{AD,MAX}$  from the externally observed values. Here,  $t, \rho, c_p$  are the layer thickness, density and specific heat capacity, respectively, of the electrocaloric layers, inner (I) and outer electrodes (O).

The term  $pT$  is treated as a constant

$$pT \approx -\rho_{cp} \frac{\Delta T_{AD,MAX}}{\Delta E_{MAX}} < 0, \quad (9)$$

to simplify the solution of the differential Eqn. 4 to linear functions instead of exponential functions, which allows a first-principle discussion. For the investigated material with  $\Delta T_{AD,MAX} \ll T_C$ , the results are not significantly influenced.

### C. ADIABATIC AND PARTIALLY NON-REVERSIBLE PHASES

The solution of Eqn. 4 for  $dQ = 0$  for increasing and decreasing field along the adiabatic paths with the initial conditions  $T(E_1) = T_C$  and  $T(E_2) = T_H$  gives the temperature as a function of the rising field ( $E = E_1 \dots E'_1$ )

$$T_1(E) = T_C + \left( \frac{\Delta T}{\Delta E} \Big|_{AD} + \frac{\Delta T}{\Delta E} \Big|_{DF} \right) (E - E_1) \quad (10)$$

and for falling field ( $E = E_2 \dots E'_2$ )

$$T_2(E) = T_H + \left( \frac{\Delta T}{\Delta E} \Big|_{AD} - \frac{\Delta T}{\Delta E} \Big|_{DF} \right) (E - E_2) \quad (11)$$

with the reversible (electrocaloric) temperature change per field change

$$\frac{\Delta T}{\Delta E} \Big|_{AD} = \frac{\Delta T_{AD,MAX}}{\Delta E_{MAX}} \quad (12)$$

and irreversible (material dissipation) temperature change per field change

$$\frac{\Delta T}{\Delta E} \Big|_{DF} = \frac{DF_{TR} \Delta E_{MAX} \frac{\pi}{8} \varepsilon_{TR}}{\rho_{cp}}. \quad (13)$$

The ratio  $r_T$  between the irreversible and reversible temperature change per field change

$$r_T = \frac{DF_{TR} \Delta E_{MAX}^2 \frac{\pi}{8} \varepsilon_{TR}}{8\rho_{cp} \Delta T_{AD,MAX}} \quad (14)$$

is defined here to simplify the following expressions.

The resulting temperature change per field change is

$$\frac{dT_1}{dE} = \frac{\Delta T}{\Delta E} \Big|_{AD} + \frac{\Delta T}{\Delta E} \Big|_{DF} > \frac{\Delta T}{\Delta E} \Big|_{AD} \quad (15)$$

$$\frac{dT_2}{dE} = \frac{\Delta T}{\Delta E} \Big|_{AD} - \frac{\Delta T}{\Delta E} \Big|_{DF} < \frac{\Delta T}{\Delta E} \Big|_{AD} \quad (16)$$

and differs from idealized isentropic ( $DF = 0$ ) phases.

For any  $E'_2$  (defined by a'), the hot temperature is now expressed by evaluation of Eqn. 11 at  $E'_2$ ;  $T_2(E'_2) = T_C$  as

$$T_H = T_C + a' \Delta T_{AD,MAX} (1 - r_T). \quad (17)$$

This result is then used to calculate the intermediate field  $E'_1$  during rising fields, required to realize the same temperature difference  $T_H - T_C$  for closed thermal cycles, by solving  $T_1(E'_1) = T_H$  for  $E'_1$  (Eqn. 10), which is

$$E'_1 = E_1 + a' \Delta E \frac{1 - r_T}{1 + r_T}, \quad (18)$$

approximately

$$E'_1 \approx E_1 + a' \Delta E (1 - 2r_T) \approx E_1 + a' \Delta E. \quad (19)$$

It is noted that the irreversible temperature increase  $\Delta T_{IRR} = T'_C - T_C$  of a fully adiabatic cycle (increasing and subsequently decreasing the field by  $\Delta E_{MAX}$ , see Fig. 6), as it is used in [16] for analysis of magnetocaloric systems, can be calculated as

$$\Delta T_{IRR} = \left( \frac{dT_1}{dE} - \frac{dT_2}{dE} \right) \Delta E = \frac{DF_{TR} \pi \varepsilon_{TR} \Delta E^2}{4\rho_{cp}}. \quad (20)$$

### D. ISOTHERMAL PHASE (COLD SIDE)

Integration of Eqn. 4 for constant temperature  $T = T_C$  along the monotonously decreasing field  $E = E'_2 \dots E_1$  gives the heat  $Q_C > 0$  absorbed from the cold side

$$Q_C = \underbrace{-pT(E'_2 - E_1)}_{>0} - \underbrace{\frac{\pi}{8} DF_{TR} \varepsilon_{TR} \Delta E (E'_2 - E_1)}_{<0}, \quad (21)$$

which is slightly less than the theoretical  $Q_{C,EC}$  of a true Carnot-cycle (assuming  $DF = 0$ ) due to the non-reversible material loss (since practically  $DF > 0$ ). However, as long as the non-reversible energy is much lower than the useful heating energy ( $W_{DF,MAX} \ll W_{EC,MAX}$ ), namely

$$\frac{\pi}{8} DF_{TR} \varepsilon_{TR} \Delta E_{MAX}^2 \ll -pT \Delta E_{MAX}, \quad (22)$$

then the cooling energy is not noticeably reduced, and approximated by

$$Q_C \approx Q_{C,EC} = -pT(E'_2 - E_1). \quad (23)$$

### 1) ELECTRICAL WORK INPUT

The total electrical work input  $W_{IN} = W_{INT} + W_{EXT}$  consists of the internal work  $W_{INT} = W_{EC} + W_{DF}$ , which is the sum of the non-zero input work  $W_{EC}$  for a useful thermodynamic cycle with  $\Delta T > 0$  and the dissipation  $W_{DF}$  within the material with  $DF > 0$  during that cycle, and the external work  $W_{EXT}$ , associated with the electrical losses of the electrical charging and discharging circuit with finite charging efficiency  $\eta < 100\%$ .

The first part of the internal work is calculated for a loss-less electrocaloric dielectric for a symmetric and triangular rising and falling electric field (the sum of both transition times is  $t_T$ , where the summed up field change of  $2\Delta E$  with slope  $\pm dE/dt$  happens), with the already calculated field dependent temperatures from Eqn. 10 and Eqn. 11 during the adiabatic phases by following a linearized method from [5], [6], [12] with  $dD = \varepsilon dE + p dT$  as

$$W_{EC} = \int_0^{t_T} E(t) \frac{dD(t)}{dt} dt = \Delta W_{EC} + \Delta W'_{EC}, \quad (24)$$

and the two resulting summands

$$\Delta W_{EC} = -pT_H(E_2 - E'_1) - p\Delta E_{1*} \cdot (T_C - \frac{\Delta E_{1*}}{2\rho_{CP}}(pT - DF_{TR}\Delta E \frac{\pi}{8}\varepsilon_{TR})) \quad (25)$$

$$\Delta W'_{EC} = pT_C(E'_2 - E_1) + p\Delta E_{2*} \cdot (T_H + \frac{\Delta E_{2*}}{2\rho_{CP}}(pT + DF_{TR}\Delta E \frac{\pi}{8}\varepsilon_{TR})) \quad (26)$$

with  $\Delta E_{1*} = E'_1 - E_1$  and  $\Delta E_{2*} = E_2 - E'_2$ . Inserting  $T_H$  from Eqn. 17 and  $E'_1$  from Eqn. 18 results in

$$W_{EC} = -p\Delta E \Delta T_{AD,MAX} a' (1 - a' + r_T) \frac{1 - r_T}{1 + r_T} \approx -p\Delta E \Delta T_{AD,MAX} a' (1 - a'), \quad (27)$$

where the approximation is for the condition from Eqn. 22.

The second part of the internal work is calculated as the material dissipation of a lossy dielectric as

$$W_{DF} = 2 \frac{\pi}{8} \Delta E_{MAX} \int_{E_1}^{E_2} \varepsilon(E) DF(E) dE = \frac{\pi}{4} DF_{TR} \varepsilon_{TR} \Delta E_{MAX}^2. \quad (28)$$

For the internal material losses, only a small fraction (dissipation factor  $DF$ ) of stored energy related to the permittivity  $\varepsilon_{TR}$  contributes, while the main part related to  $\varepsilon_{TR}$  vanishes for closed cycles, since the cycling stored energy is not dissipated. However, the charging and discharging power which has to be provided externally is linked to the total permittivity  $\varepsilon_{TR}$ , such that the external loss from a highly-efficient, but still lossy charging and discharging circuit is approximated as the additional loss term

$$W_{EXT} = (1 - \eta_{DC}) \varepsilon_{TR} \Delta E_{MAX}^2, \quad (29)$$

where  $\eta_{DC}$  is the average efficiency of the external charging circuit for providing the charging or discharging power. For simplicity, the external charging losses only consider the charging power for the real permittivity, neglecting the power for providing the pyrocurrent or material dissipation. The result is insignificantly influenced if Eqn. 22 and  $DF \ll 1$  is satisfied. For materials with significant dissipation factors (for example electrocaloric polymers, or ceramics with significant hysteresis or ferroelectric effects),  $W_{EXT}$  is further increased since the material loss power is likewise provided by the external charging circuit with additional external

charging losses. Even though these materials are out of the scope of this work, Eqn. 29 might be extended by  $DF$ .

Comparing Eqn. 28 and Eqn. 29 reveals that both the internal dissipation factor of the material ( $\frac{\pi}{4}DF$ ) and the external loss from the charging loss  $(1 - \eta_{DC})$  contribute proportionally to the required total power input. If  $DF \ll (1 - \eta_{DC})$ , which is the case here since the very low dissipation factor of the ceramic ( $\approx 0.2\%$ ) still is significantly lower than the external charging loss factor ( $\approx (1 - 99.2\%) = 0.8\%$ ), then the realistic system COP of actual heat pump systems (including the required charging circuit) will be significantly reduced compared to the theoretical material COP. The effect on the different COPs is calculated in the following.

### E. COEFFICIENT OF PERFORMANCE (COP)

The maximum possible coefficient of performance for a refrigerator heat pump with  $\Delta T = T_H - T_C$  at  $T_C$  is the Carnot COP

$$COP_{CAR} = \frac{Q_C}{W_{CAR}} = \frac{T_C}{T_H - T_C}. \quad (30)$$

To absorb the heat  $Q_C$  from the cold side, the minimum work input thus is

$$W_{CAR} = Q_C \frac{\Delta T}{T_C} \quad (31)$$

Considering a loss-free external supply of the charging and discharging power ( $W_{EXT} = 0$ ), the material COP is

$$COP_{MAT} = \frac{Q_C}{W_{INT}}, \quad (32)$$

with  $Q_C$  from Eqn. 4 and the internal input work  $W_{INT} = W_{EC} + W_{DF}$  from Eqn. 27 and Eqn. 28. The relative material

$$COP_{R,MAT} = \frac{COP_{MAT}}{COP_{CAR}} \leq 1 \quad (33)$$

expresses how close the actual thermodynamic cycle is to the ideal Carnot limit. One important optimization goal is to achieve the highest possible  $COP_R$ . Since the  $COP_R$  depends on the ratio  $a'$ , the optimal value is calculated: The maximum of  $COP_R$  is identified by solving  $\frac{d}{da'} COP_R(a') = 0$ , which gives the optimal electric field ratio

$$a'_{OPT} = \left. \frac{E_2 - E'_2}{\Delta E} \right|_{OPT} = \frac{1}{1 + \sqrt{1 + \frac{\Delta T_{AD,MAX}}{2T_C} \frac{1 - r_T}{1 + r_T}}}, \quad (34)$$

which is approximated for typical electrocaloric materials with  $\Delta T_{AD,MAX} \ll T_C$  by

$$a'_{OPT} \approx \frac{1}{2}. \quad (35)$$

Likewise, the optimal temperature ratio  $\alpha_{OPT}$  of temperature difference to the maximum adiabatic temperature change (which is used in [16] instead of the electrical field ratio  $a'$  used in this work) is

$$\alpha_{OPT} = \left. \frac{T_H - T_C}{\Delta T_{AD,MAX}} \right|_{OPT} = (1 - r_T) a'_{OPT}, \quad (36)$$

which is approximated by

$$\alpha_{\text{OPT}} \approx \frac{1}{2}. \quad (37)$$

Evaluation of the approximated form of  $COP_{\text{R}}$  using the approximated optimal electric field ratio ( $a' = \frac{1}{2}$ ) results in the first-principle description of the expected relative COP as a function of material characteristics:

$$COP_{\text{R},\text{MAT}} \approx \frac{1}{1 + \frac{4\varepsilon_{\text{TR}}T\Delta E_{\text{MAX}}^2}{\rho_{\text{CP}}\Delta T_{\text{AD},\text{MAX}}^2} \left(\frac{\pi}{4}DF_{\text{TR}}\right)}. \quad (38)$$

The expression in Eqn. 38 provides insight into the effect of the material dissipation factor  $DF$  on the material COP. For real heat pump systems, the loss from the external charging circuit have to be included in the analysis, which gives the system COP

$$COP_{\text{SYS}} = \frac{Q_{\text{C}}}{W_{\text{INT}} + W_{\text{EXT}}} \quad (39)$$

and relative system COP

$$COP_{\text{R},\text{SYS}} = \frac{COP_{\text{SYS}}}{COP_{\text{CAR}}} = \frac{W_{\text{CAR}}}{W_{\text{INT}} + W_{\text{EXT}}} \leq COP_{\text{R},\text{MAT}} \quad (40)$$

Evaluation at the approximated optimal ratio ( $a' = \frac{1}{2}$ ) results in the first-principle description of the expected relative COP as a function of internal material characteristics and the external charging efficiency:

$$COP_{\text{R},\text{SYS}} \approx \frac{1}{1 + \frac{4\varepsilon_{\text{TR}}T\Delta E_{\text{MAX}}^2}{\rho_{\text{CP}}\Delta T_{\text{AD},\text{MAX}}^2} \left(\frac{\pi}{4}DF_{\text{TR}} + (1 - \eta_{\text{DC}})\right)}. \quad (41)$$

Eqn. 41 gives insight into the required conditions to achieve a high relative system COP, similar to the discussion in the supplementary material of [12]. However, Eqn. 41 provides additional insight into the partitioning of material loss and external charging loss. To achieve the ideal Carnot COP ( $COP_{\text{R},\text{SYS}} = 1$ ), the second summand in the denominator has to vanish. However, neither the material parameters (first factor) nor the dissipation factor or electrical efficiency (second factor) can physically be zero. The summands and factors are combined into figure-of-merits and discussed in the following.

### F. FIGURE-OF-MERITS

Considering only the material losses, a performance-determining material figure-of-merit is

$$FOM_{\text{EC},\text{MAT}} = \frac{\rho_{\text{CP}}\Delta T_{\text{AD},\text{MAX}}^2}{4\varepsilon_{\text{TR}}T\Delta E^2} \frac{1}{\frac{\pi}{4}DF_{\text{TR}}} \quad (42)$$

For example, to achieve over 50% Carnot efficiency ( $COP_{\text{R},\text{MAT}} = \frac{1}{2}$ ), a  $FOM_{\text{EC},\text{MAT}} > 1$  is required. Interestingly, if only the achievable relative material  $COP_{\text{R},\text{MAT}}$  is investigated then only the product  $DF_{\text{TR}}\varepsilon_{\text{TR}}$  is important. In this pure material investigation, high COPs seem

possible for both high-permittivity materials with very low  $DF$  (for example  $< 0.2\%$ ) such as the used PMN ceramics [17] (including the one investigated in this work), and low-permittivity materials with higher  $DF$  such as polymers [18].

Including both the material loss and charging efficiency, a performance-determining system figure-of-merit is

$$FOM_{\text{EC},\text{SYS}} = \frac{\rho_{\text{CP}}\Delta T_{\text{AD},\text{MAX}}^2}{4\varepsilon_{\text{TR}}T\Delta E^2} \frac{1}{\frac{\pi}{4}DF_{\text{TR}} + (1 - \eta_{\text{DC}})}. \quad (43)$$

$=FOM_{\text{EC}} \quad =DF_{\text{SYS}}^{-1}=(1-\eta_{\text{SYS}})^{-1}$

Now it is clear that if the efficiency of the external charging circuit is much worse than the dissipation factor of the material, then the external charging efficiency  $\eta_{\text{DC}}$  in combination with the permittivity  $\varepsilon$  limits the achievable system  $COP_{\text{R},\text{SYS}}$ , and not the dissipation factor  $DF$  of the material any more. Based on this considerations, a low-permittivity material with slightly increased  $DF$  might be beneficial to achieve higher  $COP_{\text{R},\text{SYS}}$ , if the practically possible external charging efficiency is limited (for example to 99%, or 1% loss). For the combination of an ultra-low loss material dissipation factor and limited external charging efficiency ( $DF_{\text{TR}} \ll (1 - \eta_{\text{DC}})$ ) the performance-determining system figure-of-merit is bound by approximately

$$FOM_{\text{EC},\text{SYS}} < \frac{\rho_{\text{CP}}\Delta T_{\text{AD},\text{MAX}}^2}{4\varepsilon_{\text{TR}}T\Delta E^2} \frac{1}{1 - \eta_{\text{DC}}} \quad (44)$$

$=FOM_{\text{EC}}$

with a material figure-of-merit independent from the vanishing small material dissipation factor

$$FOM_{\text{EC}} = \frac{\rho_{\text{CP}}\Delta T_{\text{AD},\text{MAX}}^2}{4\varepsilon_{\text{TR}}T\Delta E^2}. \quad (45)$$

The system  $COP_{\text{R},\text{SYS}}$  for the case of a ultra-low loss material is now bound mainly by the product of material permittivity and the dominating external efficiency  $\varepsilon_{\text{TR}}(1 - \eta_{\text{DC}})$ , instead of the internal material dissipation factor  $\varepsilon_{\text{TR}}DF_{\text{TR}}$ .

### G. ESTIMATION OF ACHIEVABLE MATERIAL AND SYSTEM COEFFICIENTS OF PERFORMANCE

This work analyzes a PMN ceramic multilayer capacitor sample. Fig. 7 shows the calculated relative material and system COPs for operation from zero field to a final field ( $0 \dots E$ ) and locally around the operation point (at  $E$ ). The maximum of each COP is labeled. The calculations are based on Eqn. 38, Eqn. 41, the measured permittivity, dissipation factor and temperature lift from Fig. 4, material parameters from Table 1 and exemplary for an electrical charge recovery efficiency of 99.2%. The ratio between internal temperature change  $\Delta T_{\text{AD},\text{MAX}}$  and measured temperature change  $k_{\text{T}} = 1.123$  follows from a weighted average (Eqn. 8) of the material parameters (outer, inner electrodes and PMN layers) in the active regions and is used in the calculations.

**TABLE 1.** Data of electrocaloric lead magnesium niobate (PMN) material (from [2], heat capacity from [19]), inner (from [2]) and outer (from [20]) electrodes.

	electrocaloric PMN	electrodes		unit
		inner	outer	
density $\rho$	7950	10950	10491	$\text{kg m}^{-3}$
heat capacity $c_P$	326	238	234	$\text{J kg}^{-1} \text{K}^{-1}$
area	$21.5 \times 11$	$19 \times 10$	$19 \times 10$	$\text{mm}^2$
thickness $t$	30	2	10	$\mu\text{m}$
no. of layers $N$	10	9	2	
formula	$\text{Pb}(\text{Mg}_{1/3}\text{Nb}_{2/3})\text{O}_3$	$\text{Ag}_{70}\text{Pd}_{30}$	Ag	

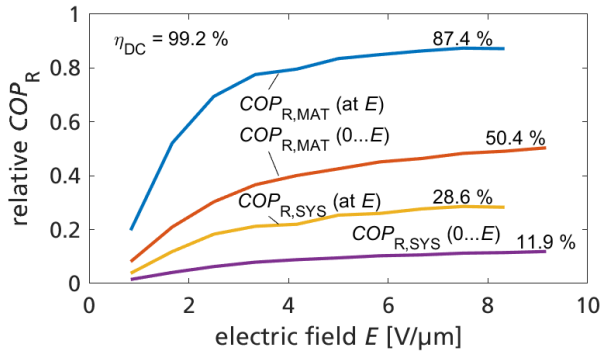


**FIGURE 7.** Calculated relative material and system COPs for operation from zero to a final field (0... $E$ ) and locally around a field (at  $E$ ).

For the conventional operation without offset (0... $E$ ), the highest material  $COP_{R,MAT} = 50.4\%$  is predicted in Fig. 7 (orange line) at operation from zero to the maximum field (here  $> 9 \text{ V } \mu\text{m}^{-1}$ ). The reason that this particular operation has the highest  $COP_{R,MAT}$  is, contrary to intuition, not because the absolute temperature lift  $\Delta T_{AD,MAX}$  is highest, if the maximum field change is used, but instead, because at higher fields the material losses increase less (due to the highly non-linear and decreasing permittivity and dissipation factor) than the increase of temperature lift. To increase the  $COP_{R,MAT}$  beyond this maximum, the high-permittivity range at lower fields should be avoided. This motivates the operation with offset fields. A theoretical case is the small-signal operation around any field (at  $E$ ). Even though the absolute temperature lift then is vanishingly small, which however could be compensated at the system level by cascading more stages at the expense of a larger system volume, the  $COP_{R,MAT}$  is significantly increased. The highest predicted material  $COP_{R,MAT} = 87.4\%$  is predicted in Fig. 7 (blue line) at operation locally (with a hypothetical vanishing small temperature change) around the field  $E = 7.5 \text{ V } \mu\text{m}^{-1}$ . The worst-case  $COP_{R,MAT} < 20\%$  occurs at operation locally around very low or zero field (but still unipolar  $E > 0$ ) because of the high losses caused by the high permittivity, although the differential temperature increase is highest around low fields. Despite the high predicted theoretical material  $COP_{R,MAT}$ , for practical systems the losses of the charging circuit have to be included in the analysis. Exemplary for a charging circuit efficiency of  $\eta_{DC} = 99.2\%$  (experimentally demonstrated later in this work), the highest

system  $COP_{R,SYS} = 11.9\%$  is predicted for operation from zero field to the maximum field. Operation locally around  $E = 7.5 \text{ V } \mu\text{m}^{-1}$  has a predicted  $COP_{R,SYS} = 28.6\%$ , which is more than doubled. The calculated relative system COPs are significantly reduced from the relative material COPs, since the assumed external charging losses (around 1%) surpass the material dissipation (below 0.2%). For practical heat pumps there is a trade-off between operation with highest cooling power (using the maximum possible field change, thus operation from zero to the maximum  $E$ ) and the highest coefficient of performance (operation locally around the optimal field  $E$ ). In between those two extrema, the preferred operation mode is from an offset field to a final field, where relative COPs between the calculated extrema are reached.

The calculations suggest that operation with offset field enables more than a doubling of the material or system COPs. However, the analysis is based on measured small-signal data, and it might be questioned if during continuous large-signal operation the measured partial temperature lift derived from the single measurement in Fig. 4 is valid. This might also be questioned since for some dielectric or magnetic materials the loss in large-signal operation is higher than expected from small-signal measurements [21]. To address this issue, this work carries out further experiments with offset fields, to verify the previously calculated results also during continuous (large-signal) operation as in a practical heat pump system.

As previously shown, the external electrical charging efficiency limits the achievable performance. While Fig. 7 was calculated for  $\eta_{DC} = 99.2\%$  efficiency, the effect of the external efficiency  $\eta_{DC}$  on  $COP_{R,SYS}$  is further investigated. Fig. 8 (solid line) shows the calculated achievable  $COP_{R,SYS}$  around the optimal  $E$  for external efficiencies up to 100%, including the measured material loss. For the ideal external efficiency of 100%, the system  $COP_{R,SYS}$  reaches the material  $COP_{R,MAT} < 100\%$ , limited only by the material losses. If the material loss is neglected ( $DF = 0$ ),  $COP_{R,MAT}$  reaches the Carnot limit (100%), as shown in Fig. 8 (dashed line). For a physical result, both the internal and external loss factors should be included in the estimation, especially if both reach very high efficiencies. Fig. 8 shows that a very high 99.71% external efficiency is required to reach above 50% of the Carnot limit. Achieving such high electrical efficiencies seems very difficult but not impossible using advanced power converter topologies and operation strategies. It should be mentioned that the external efficiency is not the only



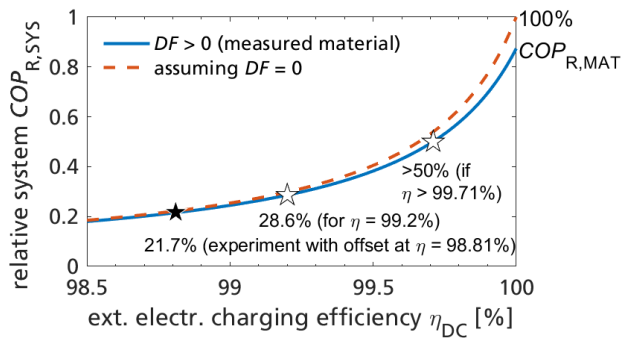


**FIGURE 8.** Calculated relative system  $COP_{R,SYS}$  as a function of external charging efficiency, including the measured material loss (solid line) at the optimal offset field, and for a loss-less material (dashed line). From continuous operation with an efficient charging circuit an operation point with offset is verified (dark star, see Table 2), which can be improved to the operation point at 99.2% electrical efficiency if more EC elements are used. For over 50% Carnot COP, at least 99.71% electrical efficiency is required.

parameter which can be improved. There are already improved electrocaloric ceramic materials available and subject to ongoing research, which show higher temperature effect at lower permittivity and field change, likewise improving the relative COP. This work uses an up to 99.2% efficient power converter as charging circuit for further experiments presented later in the paper. Using this setup, the theoretical calculated  $COP_{R,SYS} = 28.6\%$  (based on the previous small signal analysis) is experimentally verified later in this work under large signal continuous operation.

### III. EXPERIMENTAL SYSTEM COP ESTIMATION IN CONTINUOUS OPERATION

#### A. MEASUREMENT SETUP AND METHOD

A highly-efficient GaN-based half-bridge converter was built and used in this work. Fig. 9 gives an overview on the electrical setup and typical switching waveforms. The implemented hysteresis current control method for electrocaloric loads is published by the authors in [15]. The current controller is implemented on a programmable system on chip and configured by a graphical user interface (GUI). The controller generates the high-side (H) and low-side (L) control signals of the two half-bridge transistors. The input voltage  $V_{DC}$  of the converter is referenced to ground (GND). A power inductor with inductance  $L$  connects the half-bridge to the device under test (DUT), which is either a reference capacitor, or an electrocaloric capacitor. The dc-dc converter control method and parameters were carefully optimized to achieve above 99% charging efficiency (for ideal low-loss capacitors) for the complete intended operation voltage range and effective electrocaloric capacitance range.

Manual optimization of control parameters for high efficiencies resulted in the following parameters: Zero-voltage-switching (ZVS) valley current of  $-0.05$  A, ZVS peak current linearly increased from  $0.2$  A to  $0.8$  A for converter input voltages (voltage swing) of  $60$  V to  $240$  V, dead-time (valley)

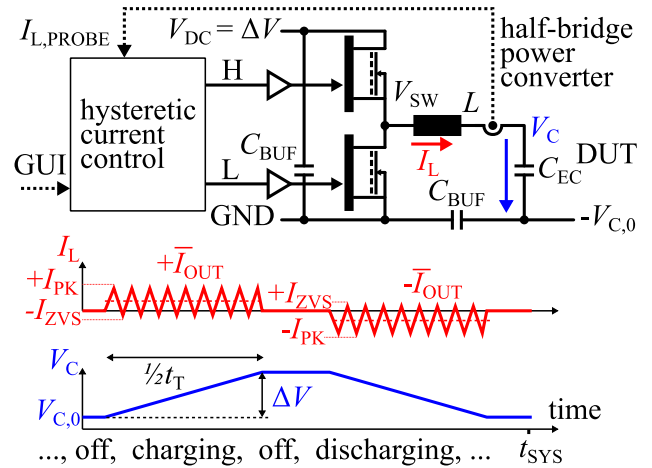


**FIGURE 9.** Schematic (top) of GaN-based switched-mode power converter with hysteretic current control, connected to electrocaloric DUT with offset voltage. Typical switching waveforms (middle). Photo of half-bridge converter (bottom).

of  $50$  ns, dead-time (peak) of  $250$  ns. To compensate for the delay of  $\approx 200$  ns of the signal and control path between the actual inductor current (measured with  $120$  MHz current probe) and the switching action (at the gates of the transistors), the current probe signal was enhanced by analog addition of a high-pass filtered signal of the current probe, with high-pass time-constant of  $\approx 200$  ns.

Fig. 10 shows exemplary switching waveforms of the inductor current, the switch-node voltage and output (load) voltage. The zoom into the switching waveforms in Fig. 11 shows the inductor current, which is kept within the peak and valley current setpoints (dashed) by the hysteretic current control. Also, the switch-node voltage is shown, where the two almost straight voltage transitions with different transition times (related to the different current setpoints prior to transistor turn-off events) are an indication of resonant and optimal ZVS switching.

To acquire a set of measurement data, the following sweeps were performed by the following nested loops, listed from the inner to the outer loop:

- cycle frequency  $f_{SYS}$ :  $\{0.25, 2, 20, 40, 80, 120, 180, 270, 405\}$  Hz

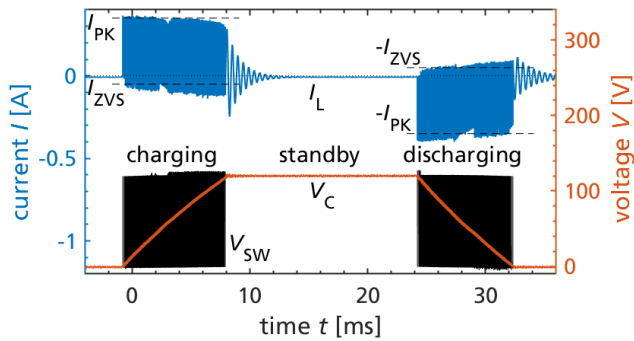


FIGURE 10. Exemplary switching waveforms (120 V, 20 Hz, 10 μF) [15].

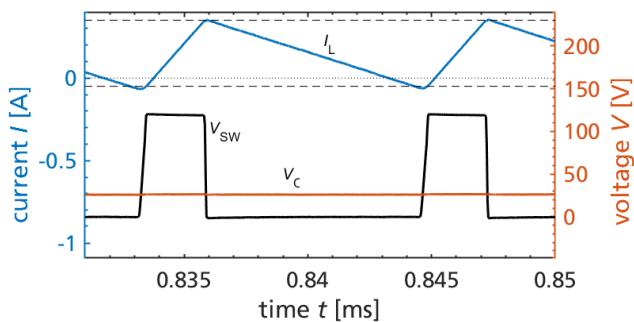


FIGURE 11. Zoom into Fig. 10 shows the hysteretic current control.

- offset voltage  $V_{C,0}$ : {0, 60, 120, 180} V
- voltage swing  $\Delta V$ : {60, 120, 180, 240} V, but only if  $V_{C,0} + \Delta V \leq 240$  V

The cycle frequency of  $f_{SYS} = 0.25$  Hz will later be used to determine the adiabatic electrocaloric temperature change of EC samples. The measurement of the power loss is impaired by the power loss of voltage probes required for the power loss measurement. This additional loss is almost independent from the cycle frequency, such that at the low 0.25 Hz frequency most of the measured power loss is not part of the converter or load losses. With increasing cycle frequency but constant charging parameters, the standby-phases between the charging and discharging times are reduced, and the measured power loss increases almost linear with increasing cycle frequency. However, the maximum possible cycle frequency is limited, because it has to be ensured that the capacitor is fully charged and discharged by  $\Delta V$  in each cycle. Since the charging time depends on the voltage swing, and the effective capacitance of the EC samples is highly bias dependent, several frequencies up to 405 Hz were measured. In the later analysis of data, for the extraction of the actual power loss it was always ensured that on the one hand a sufficiently high cycle frequency was used such that the offset losses from the probes are negligible, and on the other hand a sufficiently low cycle frequency is used such that the charging and discharging transitions are fully completed. Despite these measures, the power loss of the probes is still high. To avoid underestimation of the system performance, in the analysis of the data the power loss of the probes was calculated from

the known probe resistances (2.69 MΩ at the input from the power analyzer, 2.69 MΩ, 50 MΩ and 60 MΩ paralleled at the output from the power analyzer, oscilloscope and control system, respectively) and measured RMS voltages (from the power analyzer) and subtracted from the measured power loss prior to further calculations.

The input voltage and offset voltage are both buffered by large (compared to the capacitance of the electrocaloric samples) low-loss film capacitors (300 μF, TDK B2563xB\* MKP DC LS). Two external power supplies are used to provide the static voltage swing  $\Delta V$  and offset voltage  $V_{C,0}$ . These two supplies are connected by resistances of 1.1 kΩ, from which 100 Ω is used for the current measurement for the power analyzer. Due to the high efficiency and very low active input power of the system in continuous steady-state operation (typically around 0.1-1 mA), the external shunts were required to extend the lower end of the input range of the power analyzer (ZES LMG671). This allows measurements of the power loss with a high resolution. The combination of the large buffer capacitors and series resistances allows that the external sources only have to provide a low-pass filtered, dc-like power, which is the power loss of the system, but the around 100-times higher reactive charging and discharging power is provided and recycled by the buffer capacitors. The series resistances were only used to achieve a high accuracy of the power loss measurement, and can be omitted in real heat pump applications.

### B. REFERENCE MEASUREMENTS WITH LOW-LOSS NON-ELECTROCALORIC CAPACITORS

First, the converter was used to charge and discharge low-loss (non-electrocaloric and bias-independent) reference capacitances as device under test (DUT). Reference measurements were carried out for six different loads: 0.1 μF, 0.2 μF, 0.4 μF, 1 μF, 2 μF, 5 μF. All capacitors are metallized polypropylene film capacitors (MKP1840, 1000 V) and have a very low dissipation factor of  $\approx 0.1\%$  according to the data sheet as well as very low bias, frequency or temperature dependence.

The purpose of the reference measurements with low-loss linear capacitances is to demonstrate the high charging efficiency of the converter, and to verify that the extracted data from the measurements fits to the known capacitance values. This verification improves the confidence in the later extracted capacitance values of the samples.

Fig. 12 (top) shows the measured charging efficiency  $\eta$  for all reference capacitors and different voltage swings  $\Delta V$  (zero offset  $V_{C,0} = 0$  V, system frequency 80 Hz). Fig. 12 (bottom) shows the independence of the efficiency from non-zero offset voltages in combination with the reference capacitors. All shown power loss data include the power stage losses, but do not include the losses of the control systems and gate drivers.

For loads  $> 1 \mu\text{F}$ , over 99% efficiency is reached almost independent from the voltage swing  $\Delta V$ . The independence from the voltage swing is achieved because the peak current was linearly increased with increasing voltage swing

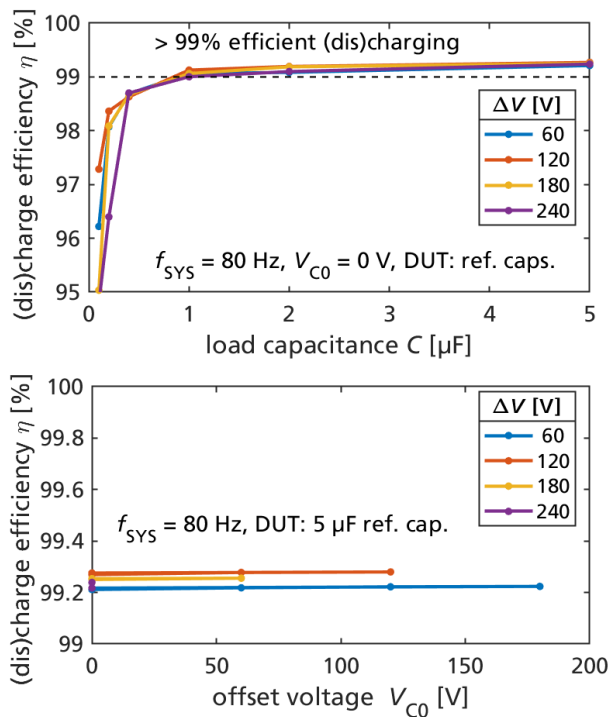


**FIGURE 12.** Measured charging efficiency for several reference capacitors and voltage swings (top) and independence from the offset voltage (bottom).

(see Sec. III-A), such that the charging time is kept constant despite different voltage swings. Increasing the peak current with increasing voltage swing also ensures that the optimal dead time (switch-node voltage transition time prior to the ZVS turn-on event) is kept almost constant, such that optimal dead times and thus low switching loss are maintained. The independence from the offset voltage (at least for the linear reference capacitors) is achieved because only the effective capacitance of the series connection of the (linear) reference capacitor and (linear) buffer capacitor is relevant for the converter power loss and independent from the offset voltage. The dependence, and low efficiency at low load capacitances  $< 1$   $\mu\text{F}$  is explained using the switching waveforms in Fig. 10 as follows: The system frequency is selected such that the capacitor is always charged and then, after a standby phase, discharged by the full voltage swing  $\Delta V$ . After the charging (or discharging) transition is finished, the voltage is kept constant during the standby phase. This (electrical) standby phase in real heat pump systems is for thermal heat transfer processes, for example between the electrocaloric material and the heat sink or source. If the system frequency is kept constant and the load capacitance is reduced as only parameter as in Fig. 12 (top), then the charging time reduces linearly with reduced load capacitance. Consequently, the ratio between charging and standby times increases. In the example in Fig. 10 this ratio is approximately 1:2. However, compared to that reference measurement with a 10  $\mu\text{F}$  load, the lowest reference capacitance of only 0.1  $\mu\text{F}$  results in a ratio of

over 1:200. For the low load capacitance the converter thus operates mainly in standby mode which is a poor utilization of the converter, and the number of switching events required to cause a full voltage transition is significantly reduced. Two main factors related to the extreme ratio cause the efficiency reduction: First, the standby losses (for example due to leakage currents in the transistors and other components) are becoming more and more relevant, ultimately even exceeding the charging losses. Second, low switching loss (ZVS operation) is achieved by the hysteretic current controller only *during* continuous switching operation of the converter, as within each charging or discharging phase. The *transition* from standby to charging or discharging however is still one transition where ZVS operation is not possible. Increased switching losses occur thus twice per cycle at the transitions from standby to charging/discharging mode. Only if the load capacitance is sufficiently high, then this total of two non optimal switching events becomes negligible compared to the thousands of optimal ZVS switching events. For real heat pump systems a standby ratio of 1:5 seems sufficient, and by paralleling many EC elements (compared to only one in this work) it is possible to avoid the operation mode with extreme standby ratios. Thus, for practical heat pump applications, a high converter utilization and high efficiency is possible.

Fig. 13 shows the measured raw (top) and corrected (bottom) power loss data from the power analyzer as a function of the cycle frequency and for different reference capacitors. The power loss increases almost linearly with frequency, and offset power loss at very low frequency is clearly visible in the raw data. Subtraction of the probe losses results in the corrected data used for further calculations. The observed reduction from a perfect linear increase of corrected power loss with increasing frequency is also expected, since the maximum cycle frequency is limited at the point where the trapezoidal voltage waveform (see Fig. 9) transitions to a triangular waveform and the contribution of the probe losses per cycle scales not perfectly linear with the cycle frequency. The measured power loss (in contrary to the energy loss per cycle) is an average over the complete cycle time, however the sum of the charging and discharging time (in which the power loss occurs) is less than the total cycle time. Nevertheless, further calculations are based on energies and thus not affected.

To later estimate the effective permittivity of the EC samples during operation, the extraction method was first verified using known reference capacitor values. The extraction method to derive the average capacitance from the power analyzer data is as followed: Using the signal processing of the power analyzer, a low-pass filtered signal of the triangular inductor current (charging current) is generated, with a filter frequency below the high switching frequency of the transistors, and above the highest cycle frequency. This filtered signal represents a microscopic average of the almost constant charging and discharging current during the triangular switching periods (see Fig. 9), which is purely positive during charging and purely negative during discharging (in contrast to the bipolar current waveform generated by the

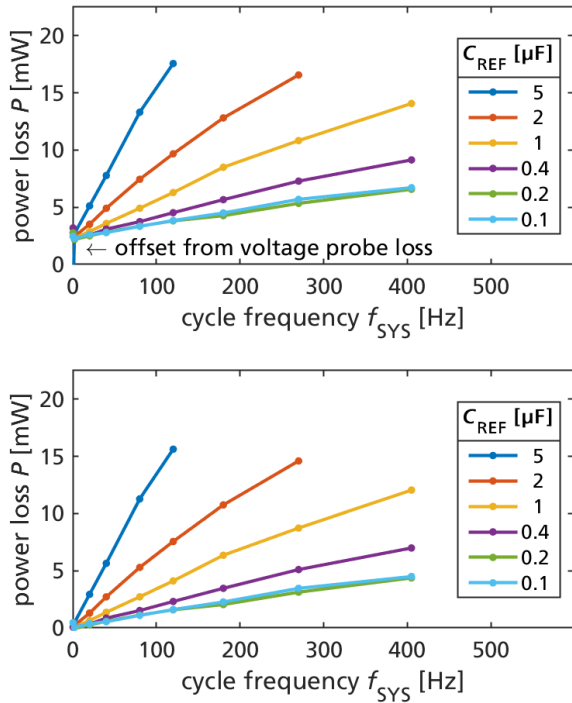


**FIGURE 13.** Measured power loss: The raw data from the power analyzer (top) is corrected by subtraction of the voltage probe losses (bottom).

current control with bipolar ZVS peak and valley currents). From this signal the average rectified value per cycle  $I_{RECT}$  is acquired. The time-related capacitance is then calculated as  $C_{TR} = I_{RECT}/(2f_{SYS}\Delta V)$ . The error of the extracted capacitance during continuous operation from the power analyzer data compared to the known reference capacitor values is below 4% for  $\geq 0.2 \mu F$ , which is the relevant range of the samples, and below 13% for  $0.1 \mu F$ .

**C. ELECTRO-THERMAL EXPERIMENTAL RESULTS IN CONTINUOUS OPERATION**

The electrocaloric multilayer-ceramic sample (Fig. 3 and Table 1) was then used as DUT and load for the converter, replacing the reference capacitor. The temperature of the sample was measured by a digitizing multimeter (DMM6500, 0.01 K resolution, 26 ms sampling time) and a type K thermocouple with low mass and thin wires (Omega CHAL-003), which was glued with a thin Kapton tape on the surface of the sample. The sample is electrically connected and mechanically clamped just on both sides, to reduce the thermal coupling to the sample holder. The adiabatic temperature change  $\Delta T_{AD,MAX}$  is extracted from the measured amplitude of the temperature waveform over one cycle during continuous steady-state operation. A slow temperature drift due to unstable environmental temperature conditions was corrected prior to the extraction by calculation of the drift of the average cycle temperature between two consecutive cycles, and subtraction of a corresponding linear temperature baseline.

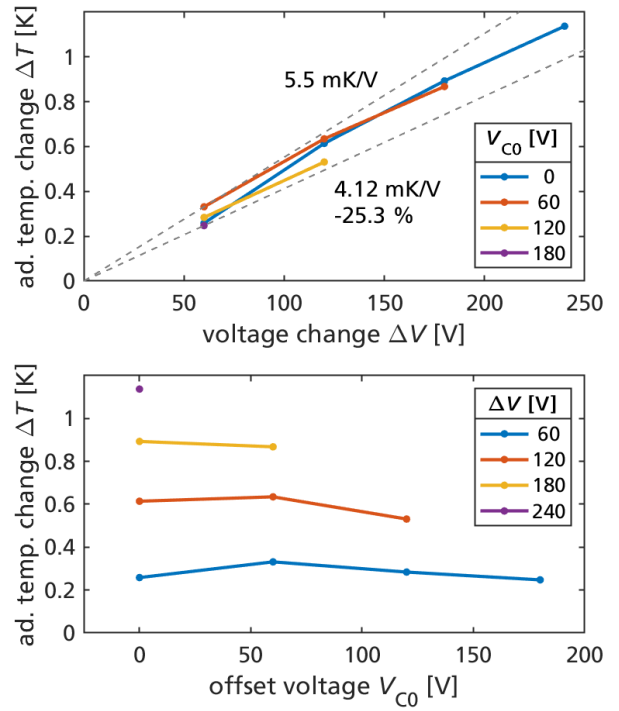


**FIGURE 14.** Measured adiabatic temperature change  $\Delta T$  depending the voltage swing  $\Delta V$  (top) and starting at different offset voltages  $V_{C,0}$  (bottom).

Fig. 14 (top) shows the measured adiabatic temperature change in continuous operation at the slowest cycle frequency of 0.25 Hz as a function of the voltage swing  $\Delta V$  and different offset voltages. The result at zero offset is consistent with the measurement in Fig. 4. The results with offset voltage demonstrates that the offset voltage has an effect on  $\Delta T$ . However, comparing the highest and lowest slopes (5.5 mK/V and 4.12 mK/V), the maximum reduction by 25.3% is still small. Fig. 14 (bottom) shows that the higher the voltage change, the higher the absolute temperature change, but on the other hand increasing the offset voltage for the same voltage change only slightly affects the temperature change. The highest  $\Delta T_{AD,MAX} \approx 1.1 K$  is lower than the highest  $\Delta T_{AD,MAX}$  from Fig. 4, because for the continuous operation the maximum voltage was reduced to 240 V (8 V/ $\mu m$ ) to avoid breakdowns.

Fig. 15 shows the effective capacitance during continuous operation, extracted as previously described from the power analyzer data. From the known geometry the effective relative permittivity is calculated and also shown. The measurement for a voltage change of  $\Delta V = 60 V$  shows that operation with offset field ( $V_{C,0} = 180 V$ ) reduced the effective permittivity by 88% compared to operation with the same  $\Delta V$  at zero offset. Compared to operation with the full voltage change of  $\Delta V = 240 V$  and zero offset, the permittivity is reduced by 71%.

The measured power loss with the electrocaloric sample is compared to the power loss with the reference capacitor. This allows a distribution of the total measured power

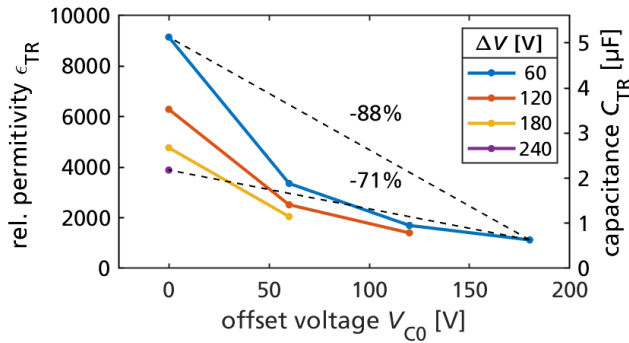


FIGURE 15. Permittivity extracted during continuous operation.

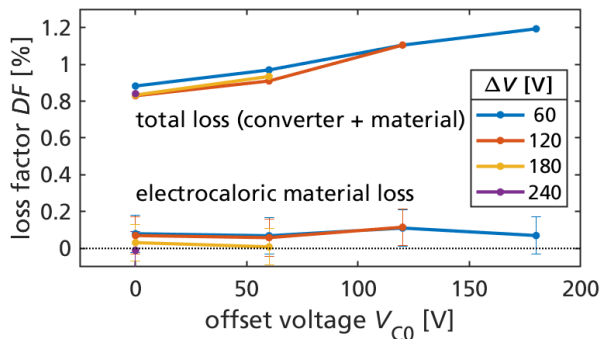


FIGURE 16. Measured total power loss shown as dissipation factor, and estimated partial contribution of the material loss.

loss into the losses from the converter and losses from the sample dissipation factor. Fig. 16 shows the measured total power loss as a dissipation factor ( $DF = 1 - \eta$ ), which is around 1%. The estimated dissipation factor of the sample is below 0.2%, consistent with the small-signal measurement in Fig. 4. Since the reference capacitor itself has a non-zero dissipation factor of around 0.1%, the estimated sample loss factor is shown with error bars ( $\pm 0.1\%$ ). It is again clearly visible that the losses of the converter significantly exceed the material losses, which will reduce the system COP.

#### D. COP ESTIMATION FROM EXPERIMENTAL RESULTS IN CONTINUOUS OPERATION

This work does not implement a real heat pump system where heat is exchanged between the sample and an external heat source or sink. Instead, the sample is operated purely adiabatic. Nevertheless, it is still possible to estimate the heat pump COP under optimal conditions as derived in the first section from the continuous operation with the power converter: From the measured temperature change at a low cycle frequency of 0.25 Hz, the adiabatic temperature change is taken as  $\Delta T_{AD,MAX}$ . The cooling energy is estimated for a Carnot-like cycle where approximately half of the measured temperature change is the expected optimal temperature difference  $T_H - T_C = \frac{1}{2} \Delta T_{AD,MAX}$  as  $Q_C \approx \frac{1}{2} \Delta T_{AD,MAX} \rho_{CP} \nu$  with the volume  $\nu$  of the electrocaloric active part of the

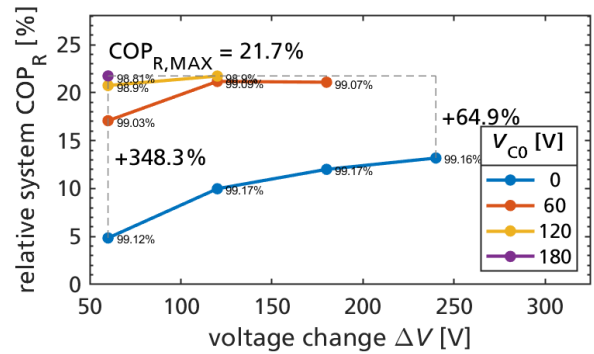


FIGURE 17. Estimated achievable relative system ( $COP_{R,SYS}$ ) for different offset voltages and voltage steps (at room temperature). Small labels: Charging efficiency  $\eta_{DC}$ .

MLCC component. From the measured total power loss  $P_{IN}$  (input power of the converter, corrected for the probe losses) at a high cycle frequency of  $f_{SYS} = 80$  Hz, the power loss per cycle is taken as  $W_{EXT+INT} = \frac{P_{IN}}{f_{SYS}}$ . The theoretical absolute Carnot-COP is calculated as  $COP_{CAR} = \frac{T}{\frac{1}{2} \Delta T_{AD,MAX}}$ , and the minimum work input for a Carnot cycle to realize the cooling energy as  $W_{CAR} = Q_C \frac{\frac{1}{2} \Delta T_{AD,MAX}}{T}$ . The achievable absolute system COP is estimated as  $COP_{SYS} = \frac{Q_C}{W_{EXT+INT} + W_{CAR}}$  and the achievable relative system COP as  $COP_R = \frac{COP_{SYS}}{COP_{CAR}}$ .

Fig. 17 shows the estimated achievable relative system COP for different operation points. The measurement for a voltage change of  $\Delta V = 60$  V shows that operation with offset field ( $V_{C,0} = 180$  V) improves the  $COP_{R,SYS}$  from 4.85% by +348.3% to 21.7%, compared to operation with the same  $\Delta V$  at zero offset. Compared to operation with the full voltage change of  $\Delta V = 240$  V and zero offset ( $COP_{R,SYS} = 13.19\%$ ), the improvement is still +64.9%.

The offset field improves on the one hand the relative performance, but on the other hand reduces the available temperature change and thus cooling power. The system still consists of the same volume of the material, such that the power density (utilization) of the system is reduced. This trade-off between performance and power density is shown in Fig. 18 as a function of  $\Delta T$  (top figure) and as a function of the heat absorbed by the one electrocaloric element (bottom figure). The figure also shows the pareto front, which consists of possible optimal solutions for the trade-off between performance and power density. For example, a reasonable operation strategy of an actual heat pump prototype might not be at the highest performance of  $COP_{R,SYS} \approx 21.7\%$  with a low cooling energy of just 18.3 mJ ( $\Delta T = 0.124$  K) per element and cycle, but instead at a slightly reduced performance of  $COP_{R,SYS} \approx 21.1\%$  with significantly higher cooling energy of 64.1 mJ ( $\Delta T = 0.434$  K).

The previous measurements were at room temperature. Further measurements were carried out over an environment temperature range of  $\approx 15 \dots 50$  °C (the sample and sample holder was heated on a temperature plate). The four data points on the pareto front, which are for different offset

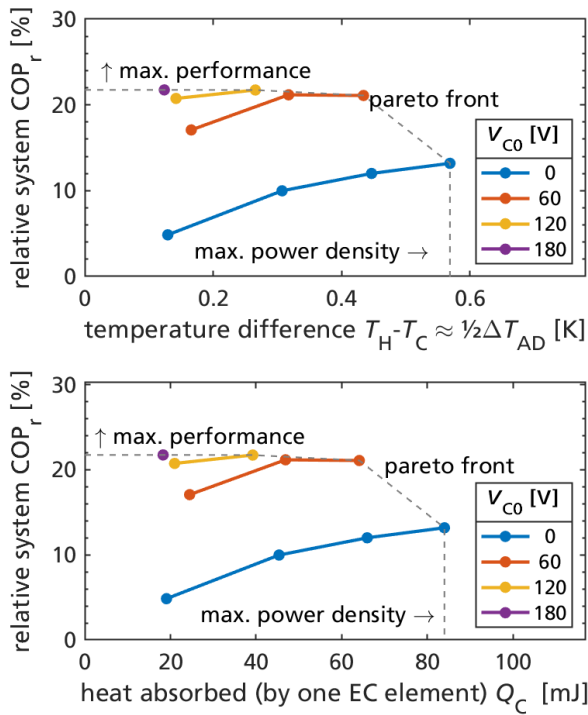


FIGURE 18. Trade-off between performance ( $COP_{R,sys}$ ) and power density (at room temperature). Top:  $\Delta T$ , bottom: absolute heat absorbed  $Q_C$ .

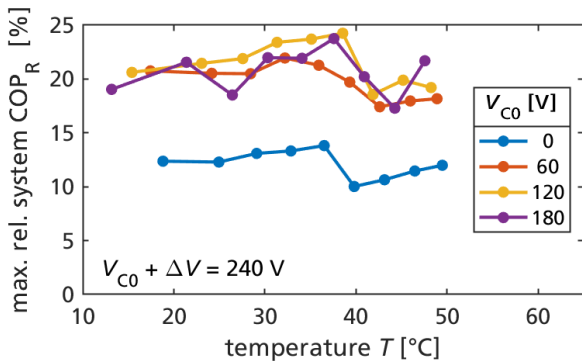


FIGURE 19. Measurement over a wide environmental temperature range.

voltages, but always with a final voltage of 240 V, are shown in Fig. 19 as a function of temperature. This temperature sweep shows that a similarly high relative COP, and an improvement by using the offset field, is achieved over a wide range of temperature, required for example for air conditioners.

IV. DISCUSSION

A. DISCUSSION AND COMPARISON WITH THE STATE-OF-THE-ART

While there are already many publications on electrocaloric materials as part of over decades of material research [18], there are only few which demonstrate actual heat pump prototypes. Comprehensive overviews of electrocaloric prototypes

are found in [22] and [23]. This work only compares the results to the few works which either use efficient charging circuits (in contrast to many works with zero energy recovery, which is often used for pure material characterization) or use offset fields.

From published prototypes, to the best of the author’s knowledge, only the works [7], [8] use *efficient charging circuits* in an attempt to maintain a high performance also on the system level. In [8] and [7] two variations of resonant circuits are used and achieve up to 80% charging efficiency. This work achieves over 99% charging efficiency, and thus is a 20-fold improvement compared to the state-of-the-art charging circuits used today for electrocaloric prototypes. The lower efficiency of the resonant circuits results partially from diode conduction losses (which is avoided in this work by the ohmic conduction of field effect transistors), and furthermore because in resonant circuits the required inductance is linked by the desired resonance frequency to the absolute value of the electrocaloric capacitance as well as the charging current and time. This results in either high charging currents with excessive conduction loss in the inductors, or in high inductance values, which increase the series resistances and thus again cause high conduction loss and limited efficiency. This work’s switched-mode power converter approach avoids the limitations of resonant circuits, and allows an independent dimensioning of the charging time, current and thus an significant improvement of efficiency. Furthermore the approach presented in this work allows arbitrary voltage waveforms (demonstrated by the authors in [15]), for example to realize arbitrary field variation [24]. This work also allows to split the charging and discharging voltage transitions into two partial voltage transitions, for example to first quickly increase the field by around half of the maximum field change (adiabatic phases of Carnot-cycle) and then to further slowly increase the field to the final field value (isothermal phases of Carnot-cycle). The control of the converter also allows to synchronize the voltage waveform to mechanical actuation waveforms, for example if mechanical movement of electrocaloric elements is used to realize thermal diodes [8].

In the work [8], in addition to using efficient resonant-circuit charging circuits, it was experimentally demonstrated that *offset fields* improve the overall COP. The barium titanate ( $BaTiO_3$ ) ceramic in [8] has a similar non-linear decrease of permittivity with applied field, while the temperature effect is only reduced slightly. The observed COP improvement with increasing offset field can be explained by the analysis in this work. Even though [8] reports a significant improvement of the absolute COP from 8.4 to 14 by using an offset field (maintaining the final field), which is an improvement by +67%, the offset also reduced the temperature lift from 0.26 K to 0.175 K. As mentioned in [22], on the system level a multistage approach can scale up the overall temperature span of the systems, and the overall performance then is more comparably described by the relative COP compared to the Carnot limit. Calculation of the relative COPs shows that the relative system COP is still improved, but only by +12%.

**TABLE 2.** State-of-the-art comparison of this work to two works using either efficient charging circuits or offset fields. Notes: (A) half of measured maximum adiabatic temperature change  $\approx \frac{1}{2} \Delta T_{AD,MAX}$ , (B) percent of the final voltage, (C) calculated as explained in this paper (D) relative improvement of  $COP_{R,SYS}$  by the offset field compared to zero offset. (E) Predicted if ten paralleled components are used to operate in the highly efficient load range of the converter.

reference	material	$\eta_{DC}$	$\Delta T$ [K]	$COP_{SYS}$	$COP_{CAR}$	$COP_{R,SYS}$	offset <sup>B</sup>	improvement <sup>D</sup>
Meng'20 [7]	P(VDF-TrFE-CFE)	70%	6	5.8	48	12.1%	0%	
Defay'18 [8]	BaTiO <sub>3</sub>	0%	0.26	2.9	1146	0.25%	0%	
Defay'18 [8]	BaTiO <sub>3</sub>	80%	0.26	8.4	1146	0.73%	0%	
Defay'18 [8]	BaTiO <sub>3</sub>	80%	0.175	14	1703	0.82%	23%	+12%
this work	PMN	99.16%	0.569 <sup>A</sup>	69	525	13.2% <sup>C</sup>	0%	
this work	PMN	99.07%	0.434 <sup>A</sup>	145	688	21.1% <sup>C</sup>	25%	+60%
this work	PMN	98.90%	0.266 <sup>A</sup>	244	1124	21.7% <sup>C</sup>	50%	+64%
this work	PMN	98.81%	0.124 <sup>A</sup>	524	2410	21.7% <sup>C</sup>	75%	+64%
this work	PMN	(99.2% <sup>E</sup> )	0.124 <sup>A</sup>	(689 <sup>E</sup> )	2410	(28.6% <sup>E</sup> )	75%	(+117% <sup>E</sup> )

Nevertheless, [8] so far is the only work prior to this work which beneficially combines an efficient charging circuit with offset fields for electrocaloric cooling, both improving the relative COP. In this work the offset field improved the relative COP by +64%, and thus is, in addition to the improvement by the high charging efficiency, another significant improvement compared to the state-of-the-art.

Table 2 compares this work to the works [7], [8] in terms of the charging efficiency and improvement of the relative COP, based on measured (and estimated) temperature difference  $\Delta T$ , measured (and estimated) absolute system COP, absolute Carnot COP to realize  $\Delta T$  and relative system COP. The offset field is listed as percent of the final field value.

## B. POSSIBLE IMPROVEMENTS AND OUTLOOK

Based on the results in Fig. 8 for the investigated electrocaloric ceramic PMN material, the required charging efficiency for an above 50% relative COP is 99.71%. Compared to the maximum achieved charging efficiency of 99.2% in this work, a further improvement of the converter efficiency by around 3 times is required. Conventional power electronics converters using simple topologies like the half-bridge used in this work have typically efficiencies limited somewhere around or slightly above this work's efficiency. To further increase the charging efficiency, advanced highly-efficient converter topologies might be developed optimized for electrocaloric applications. Since the efficiency of 99.2% in this work already is high, a further 3-times improvement of just the converter seems very challenging. Nevertheless, the charging circuit is not the only parameter influencing the relative system COP. Further improved electrocaloric material properties will also contribute to improve the achievable relative COP. This work exemplary used a PMN ceramic, but there are already improved materials available and in ongoing research. Furthermore, the EC sample was not operated up to its breakdown voltage, such that operation up to even higher voltages might further improve the COP. The geometry of the MLCC can be further improved by reducing the thickness of the electrodes and the outer inactive areas. This work did not include heat regeneration. As discussed in [5], the

combination of the electrocaloric temperature effect with additional heat regeneration (for example by addition of heat exchangers to the system), enables a further significant improvement of the relative COP, and can be beneficially combined with the approach from this paper. This work characterized just one EC element, such that the absolute capacitance is low, and the converter is not fully utilized. For example, the operation point with the highest  $COP_{R,SYS}$  had  $C < 0.5 \mu F$ , such that the converter operated with 98.81% below the maximum efficiency of up to 99.2%. If ten paralleled components were used instead of only one, the load capacitance of around  $5 \mu F$  will allow 99.2% efficiency (see Fig. 12). In that case, a further increased  $COP_{R,SYS}$  of 28.6% is predicted (see additional data point in Fig. 8 and Table 2). The designed converter is capable of charging a significant higher amount of paralleled EC elements, and also capable of providing a higher charging current (factor 10), which will both be required for large-scale heat-pumps with a useful absolute cooling power and temperature span. It is estimated that at a cycle frequency of 20 Hz (possible in heat pumps due to the low thermal time constant of the thin component) and for a field change of 180 V at 60 V offset (trade-off on the pareto front), with charging current scaled to 8 A, a capacitance of 1.1 mF can be charged with very high efficiency, which equals around 957 EC elements (1.1  $\mu F$  at the trade-off offset field). These elements can be arranged partly in a series connection to increase the temperature span of a heat-pump, and in a parallel connection to increase the cooling power. While the COP will be further improved by both material improvement and power converter innovations, the absolute cooling power can be increased into the kilowatts range by scaling the power converter. Innovation in power electronics which already occurred for highly efficient photovoltaic inverters [11] is expected to continue for highly efficient electrocaloric heat pumps.

## V. SUMMARY

### A. CONTRIBUTIONS

The three main contributions of this work and differences compared to literature are summarized in the following.

First, this work's analysis allows a first-principle estimation of the achievable system coefficient of performance  $COP_{R,SYS}$  of electrocaloric heat pumps, including a loss breakdown between the contributions of the internal material loss (dissipation factor  $DF$ ) and external charging loss (charging circuit efficiency  $\eta_{DC}$ ). Compared to literature, this first-principle results provide new insight into the importance of highly efficient external charging circuits especially for ultra-low loss materials such as the investigated PMN ceramic.

Second, this work, utilizes a highly efficient (up to 99.2%) switched-mode power converter for the first time as charging circuit for electrocaloric components. This approach reduces the external charging losses 20 times compared to resonant-circuits used so far for electrocaloric prototypes. This significant electrical efficiency improvement results in a significant improvement of the expected system coefficient of performance of emerging electrocaloric heat pumps, and paves the way for competitive and possibly superior cooling performance compared to state-of-the-art vapor compression systems.

Third, while in literature it was already observed that offset fields improve the coefficient of performance of electrocaloric samples, this work explains this effect based on the measured non-linear decreasing capacitance-voltage dependence. The required external charging power and thus losses for operation with an offset reduced more than the reduction of the measured electrocaloric temperature effect. Even though an increased offset field at constant maximum field reduces the amplitude of the electrocaloric temperature change, it is quantified that the relative system coefficient of performance still is significantly improved, over 64% in this work.

## B. CONCLUSION

It was shown that to harness the high theoretical cooling performance of electrocaloric materials also in heat pumps on the system level, the power loss from the material dissipation and external charging loss has to be minimized. This work addressed this issue by using an over 99% efficient switched-mode power converter, reducing external charging losses compared to the state-of-the-art circuits used in electrocaloric prototypes (80% efficient) by around 20 times. Furthermore, utilization of offset fields to avoid the high-permittivity range of the non-linear field-dependence was experimentally demonstrated to further improve the relative coefficient of performance; here up to 64% for the analyzed PMN material. The combination of the highly efficient charging circuit and offset fields contributes to improve the system performance of future electrocaloric heat pumps. To achieve competitive performance with today's vapor-compression heat pumps, both the electrocaloric material properties and electrical charging efficiency is still part of ongoing research, such that not only improved materials but also innovative power converter topologies are expected to further significantly improve the system performance of

electrocaloric heat pumps. While this work analyzed a PMN ceramic, different ceramic materials (barium titanate [25] or lead scandium tantalate [26]) and polymers [18] are also available and part of ongoing research for electrocaloric cooling. Since the dielectric material properties of polymers and different ceramics significantly varies, today it seems still unclear which material system in the end will be most beneficial for actual heat pumps on the system level. While this work analyzed low-loss high-permittivity electrocaloric PMN ceramics, the experimental approach should also be applied to different ceramics and higher-loss but low-permittivity polymers, and then compared on the heat pump system level.

Open problems for future works include to demonstrate large-scale electrocaloric prototypes with a high absolute temperature span ( $>30$  K) within a wide operation temperature range (including below  $0^\circ\text{C}$ ) and cooling power ( $>1$  kW). While this work aimed to increase efficiency and performance, another research direction is to increase the power density of the system by significantly increasing the cycle frequency. However, this is limited by the thermal time constants of the geometry of the electrocaloric components, and thus requires further innovation in the layout and design of electrocaloric components. A third research direction is to consider system cost and long time reliability, both required for market penetration. Since the operation principle of the electrocaloric heat pump requires alternating thermal connection to a heat source and sink, the actual implementation of these thermal valves, for example by mechanical systems, is still a challenge.

Since the theoretically achievable material performance and heat pump system performance can exceed that of state-of-the-art vapor compression systems, and electrocaloric heat pumps are feasible without harmful refrigerants and with zero global warming potential, more extensive and multidisciplinary research on electrocaloric materials, power converters as charging circuits, and heat pump systems is considered worthwhile for an energy-efficient and emission-free future.

## REFERENCES

- [1] S. Kar-Narayan and N. D. Mathur, "Predicted cooling powers for multilayer capacitors based on various electrocaloric and electrode materials," *Appl. Phys. Lett.*, vol. 95, no. 24, 2009, p. 242903.
- [2] C. Molin, P. Neumeister, H. Neubert, and E. Sylvia Gebhardt, "Multilayer ceramics for electrocaloric cooling applications," *Energy Technol.*, vol. 6, no. 8, pp. 1543–1552, 2018.
- [3] B. Nair, T. Usui, S. Crossley, S. Kurdi, G. G. Guzmán-Verri, X. Moya, S. Hirose, and N. D. Mathur, "Large electrocaloric effects in oxide multilayer capacitors over a wide temperature range," *Nature*, vol. 575, no. 7783, pp. 468–472, Nov. 2019.
- [4] J. Shi, D. Han, Z. Li, L. Yang, S.-G. Lu, Z. Zhong, J. Chen, Q. M. Zhang, and X. Qian, "Electrocaloric cooling materials and devices for zero-global-warming-potential, high-efficiency refrigeration," *Joule*, vol. 3, no. 5, pp. 1200–1225, May 2019.
- [5] U. Plaznik, M. Vrabelj, Z. Kutnjak, B. Malič, A. Poredoš, and A. Kitanovski, "Electrocaloric cooling: The importance of electric-energy recovery and heat regeneration," *EPL (Europhys. Lett.)*, vol. 111, no. 5, p. 57009, 2015.



- [6] D. E. Schwartz, "Thermodynamic cycles and electrical charge recovery in high-efficiency electrocaloric cooling systems," *Int. J. Refrig.*, vol. 131, pp. 970–979, Nov. 2021.
- [7] Y. Meng, Z. Zhang, H. Wu, R. Wu, J. Wu, H. Wang, and Q. Pei, "A cascade electrocaloric cooling device for large temperature lift," *Nature Energy*, vol. 5, no. 12, pp. 996–1002, Dec. 2020.
- [8] E. Defay, R. Faye, G. Despesse, H. Strozyk, D. Sette, S. Crossley, X. Moya, and N. D. Mathur, "Enhanced electrocaloric efficiency via energy recovery," *Nature Commun.*, vol. 9, no. 1, p. 1827, Dec. 2018.
- [9] G. Sebald, E. Lefevre, and D. Guyomar, "Pyroelectric energy conversion: Optimization principles," *IEEE Trans. Ultrason., Ferroelectr., Freq. Control*, vol. 55, no. 3, pp. 538–551, Mar. 2008.
- [10] C. Chen, M. Liu, and Y. Wang, "A dual stage low power converter driving for piezoelectric actuator applied in micro mobile robot," *Appl. Sci.*, vol. 8, no. 9, p. 1666, 2018.
- [11] B. Burger and D. Kranzer, "Extreme high efficiency PV-power converters," in *Proc. 13th Eur. Conf. Power Electron. Appl.*, Sep. 2009, pp. 1–13.
- [12] Y. Wang, Z. Zhang, T. Usui, M. Benedict, S. Hirose, J. Lee, J. Kalb, and D. Schwartz, "A high-performance solid-state electrocaloric cooling system," *Science*, vol. 370, no. 6512, pp. 129–133, Oct. 2020.
- [13] A. Torelló, P. Lheritier, T. Usui, Y. Nouchokgwe, M. Gérard, O. Bouton, S. Hirose, and E. Defay, "Giant temperature span in electrocaloric regenerator," *Science*, vol. 370, no. 6512, pp. 125–129, Oct. 2020.
- [14] Y. Meng, J. Pu, and Q. Pei, "Electrocaloric cooling over high device temperature span," *Joule*, vol. 5, no. 4, pp. 780–793, 2021.
- [15] S. Moench, K. Mansour, R. Reiner, M. Basler, P. Waltereit, R. Quay, C. Molin, S. Gebhardt, D. Bach, R. Binninger, and K. Bartholomé, "A GAN-based DC-DC converter with zero voltage switching and hysteretic current control for 99% efficient bidirectional charging of electrocaloric capacitive loads," in *Proc. PCIM Eur.; Int. Exhib. Conf. Power Electron., Intell. Motion, Renew. Energy Energy Manage.*, to be published, 2022.
- [16] T. Hess, L. M. Maier, N. Bachmann, P. Corhan, O. Schäfer-Welsen, J. Wöllenstein, and K. Bartholomé, "Thermal hysteresis and its impact on the efficiency of first-order caloric materials," *J. Appl. Phys.*, vol. 127, no. 7, 2020, Art. no. 075103.
- [17] C. Molin, M. Sanlialp, V. V. Shvartsman, D. C. Lupascu, P. Neumeister, A. Schönecker, and S. Gebhardt, "Effect of dopants on the electrocaloric effect of 0.92 Pb(Mg<sub>1/3</sub>Nb<sub>2/3</sub>)O<sub>3</sub>-0.08 PbTiO<sub>3</sub> ceramics," *J. Eur. Ceram. Soc.*, vol. 35, no. 7, pp. 2065–2071, 2015.
- [18] B. Neese, B. Chu, S.-G. Lu, Y. Wang, E. Furman, and Q. M. Zhang, "Large electrocaloric effect in ferroelectric polymers near room temperature," *Science*, vol. 321, no. 5890, pp. 821–823, 2008.
- [19] H. Uršič, M. Vrabelj, L. Fulanovič, A. Brađeško, S. Drnovšek, and B. Malič, "Specific heat capacity and thermal conductivity of the electrocaloric (1-x) Pb(Mg<sub>1/3</sub>Nb<sub>2/3</sub>)O<sub>3</sub>-xPbTiO<sub>3</sub> ceramics between room temperature and 300°C," *Informacije Midem*, vol. 45, no. 4, pp. 260–265, 2015.
- [20] *MatWeb Material Property Data—Silver, Ag, 2022-02-08T15:40:16.000Z*, MatWeb, LLC Kraft Drive Suite, Blacksburg, VA 24060, USA, 2022. [Online]. Available: <https://www.matweb.com/search/DataSheet.aspx?MatGUID=63cbd043a31f4f739ddb7632c1443d33>
- [21] D. Neumayr, D. Bortis, J. W. Kolar, M. Koini, and J. Konrad, "Comprehensive large-signal performance analysis of ceramic capacitors for power pulsation buffers," in *Proc. IEEE 17th Workshop Control Modeling Power Electron. (COMPEL)*, Piscataway, NJ, USA, Jun. 2016, pp. 1–8.
- [22] A. Torelló and E. Defay, "Electrocaloric coolers: A review," *Adv. Electron. Mater.*, Dec. 12, 2022, Art. no. 2101031. [Online]. Available: <https://onlinelibrary.wiley.com/doi/full/10.1002/aelm.202101031>, doi: 10.1002/aelm.202101031.
- [23] A. Greco and C. Masselli, "Electrocaloric cooling: A review of the thermodynamic cycles, materials, models, and devices," *Magnetochemistry*, vol. 6, no. 4, p. 67, 2020.
- [24] S. Crossley, B. Nair, R. W. Whatmore, X. Moya, and N. D. Mathur, "Electrocaloric cooling cycles in lead scandium tantalate with true regeneration via field variation," *Phys. Rev. X*, vol. 9, no. 4, 2019, Art. no. 041002.
- [25] Y. D. Wang, S. J. Smullin, M. J. Sheridan, Q. Wang, C. Eldershaw, and D. E. Schwartz, "A heat-switch-based electrocaloric cooler," *Appl. Phys. Lett.*, vol. 107, no. 13, 2015, Art. no. 134103.
- [26] Y. V. Sinyavsky, N. D. Pashkov, Y. M. Gorovoy, G. E. Lugansky, and L. Shebanov, "The optical ferroelectric ceramic as working body for electrocaloric refrigeration," *Ferroelectrics*, vol. 90, no. 1, pp. 213–217, 1989.



**STEFAN MOENCH** (Member, IEEE) received the M.Sc. degree in electrical engineering and information technology from the University of Stuttgart, Germany, in 2014. He defended his doctoral thesis, in 2021. He was an Academic Research Assistant at the Institute of Robust Power Semiconductor Systems ILH. Currently, he is a Researcher of microelectronics with the Fraunhofer Institute for Applied Solid State Physics IAF, Freiburg, Germany. His research interests include highly-integrated, highly-efficient, and fast-switching GaN-based power electronics for applications such as electromobility and renewable energy conversion.



**RICHARD REINER** received the M.Sc. degree in electrical engineering from the Technical University of Berlin, Berlin, Germany, in 2007, and the Dr.-Ing. degree from the Technical University of Freiburg, in 2017. From 2007 to 2010, he was a Research Associate with the Hahn-Schickard-Gesellschaft, Institute for Microsystem Technology, Villingen-Schwenningen, where he worked on developing electronic sensor systems. Since 2010, he has been a Research Associate with the Fraunhofer Institute for Applied Solid State Physics IAF, Freiburg, on the development and characterization of GaN-based devices and circuits for power-electronic applications. He has authored or coauthored more than 100 publications.



**PATRICK WALTEREIT** received the Ph.D. degree in physics from the Humboldt-University Berlin, in 2001, on growth and characterization of non-polar oriented GaN/AlGaN hetero structures. He was a Postdoctoral Researcher at the University of California at Santa Barbara, USA, from 2001 to 2004, investigating MBE growth for GaN-based electronic and optoelectronic devices. Since 2004, he has been with the Fraunhofer IAF in Freiburg, Germany, working on GaN based high voltage and high frequency devices. Currently he is a Group Leader with the III-V Technology Department and the Deputy Head of the Power Electronics Business Unit.



**CHRISTIAN MOLIN** received the Diploma degree in chemistry from the Technical University Chemnitz, Germany, in 2012, and the Ph.D. degree for thesis on the development of perovskite-type ceramics and device structures for electrocaloric applications, in 2019. Since 2013, he has been a Research Scientist with the Department of Smart Materials and Systems, Fraunhofer Institute for Ceramic Technologies and Systems IKTS, Dresden, Germany. His research interests include ferroelectric and electrocaloric material development and components based on multilayer technology.



**SYLVIA GEBHARDT** received the Diploma degree, in 1996 and the Ph.D. degree, in 2000 for her thesis on development and characterization of fine-scaled 1-3 piezocomposites for ultrasonic transducers. She studied material science at the Technical University Bergakademie, Freiberg, Germany and at Leeds University, U.K. She is a Senior Research Scientist and the Head of the Multifunctional Materials and Components Group with the Fraunhofer IKTS, Institute for Ceramic Technologies and Systems, Dresden, Germany. Her research interests include synthesis and characterization of ferroelectric, piezoelectric, and electrocaloric materials, and development of ceramic components based on thick films, multilayers, microstructures, fibers, and composites for capacitors, sensors, actuators, and ultrasonic transducers.



**DAVID BACH** received the M.Sc. (Eng.) degree in bionik/biomimetics in energy systems from Baden-Wuerttemberg Cooperative State University (DHBW), Friedrichshafen, Germany, the master's degree from the University of Applied Sciences, Villach, Austria, and the Ph.D. degree in bioinspired optimization of oil pumps for mobile hydraulic applications from the Albert-Ludwigs-University of Freiburg, Germany, in 2017. He worked three years as a Development Engineer at the Powertrain Division, ZF Sachs AG. Since 2017, he has been a Researcher with the Department of Thermal Energy Converters, Fraunhofer IPM. His research interests include thermoelectrics and calorics.



**ROLAND BINNINGER** received the M.Sc. degree in microsystem engineering from the Albert-Ludwigs-University of Freiburg, Germany, in 2013. He was a Research Assistant at Fraunhofer Institute of Physical Measurement Techniques IPM, Freiburg, where he wrote his bachelor's and master's thesis in the areas of thermoelectric and gas measurement. He worked one year at the F&E Department of Yasunaga, Japan, and four years as a Retrofit Project Manager at Glatt Group, Binzen, Germany. Since 2019, he has been a Researcher with the Department of Thermal Energy Converters, Fraunhofer IPM.



**KILIAN BARTHOLOMÉ** received the Diploma and Ph.D. degrees in physics from the University of Freiburg. He was at the Fraunhofer Institute for Physical Measurement Techniques IPM, in 2009, where he has been the Head of the Caloric Systems Group, since 2015. His research interest includes the development of highly energy-efficient caloric cooling systems with very large cooling power density.

...